Back Cover: Visualizing an Ultra-Weak Protein-Protein Interaction in Phosphorylation Signaling (Angew. Chem. Int. Ed. 43/2014)

ARTICLE *in* ANGEWANDTE CHEMIE INTERNATIONAL EDITION · OCTOBER 2014

Impact Factor: 11.26 · DOI: 10.1002/anie.201405976

NMR spectroscopy | Hot Paper

DOI: 10.1002/anie.201405976

Visualizing an Ultra-Weak Protein–Protein Interaction in Phosphorylation Signaling**

Qiong Xing, Peng Huang, Ju Yang, Jian-Qiang Sun, Zhou Gong, Xu Dong, Da-Chuan Guo, Shao-Min Chen, Yu-Hong Yang, Yan Wang, Ming-Hui Yang, Ming Yi, Yi-Ming Ding, Mai-Li Liu, Wei-Ping Zhang, and Chun Tang**

Abstract: *Proteins interact with each other to fulfill their functions. The importance of weak protein–protein interactions has been increasingly recognized. However, owing to technical difficulties, ultra-weak interactions remain to be characterized. Phosphorylation can take place via a $K_D \approx 25$ mM interaction between two bacterial enzymes. Using paramagnetic NMR spectroscopy and with the introduction of a novel Gd^{III}-based probe, we determined the structure of the resulting complex to atomic resolution. The structure accounts for the mechanism of phosphoryl transfer between the two enzymes and demonstrates the physical basis for their ultra-weak interaction. Further, molecular dynamics (MD) simulations suggest that the complex has a lifetime in the micro- to millisecond regimen. Hence such interaction is termed a fleeting interaction. From mathematical modeling, we propose that an ultra-weak fleeting interaction enables rapid flux of phosphoryl signal, providing a high effective protein concentration.*

A protein interacts with its partner proteins to fulfill its functions and to establish its identity in cell. Though tens of thousands of protein–protein interactions have been predicted,[1] many of the interactions have never been experimentally validated. This can be due to that the interactions are too weak to be visualized with standard techniques.[2] Indeed, among the thousands of atomic resolution structures determined for protein–protein complexes, most of them are tightly bound with the binding affinity K_D values below 1 μM, and only a small fraction is in the weak-binding regimen with the K_D above 1 μM.[3] Notwithstanding, weak protein–protein interactions are involved in cell signaling and many important cellular processes. How proteins weakly interact is of great biological and chemical interest.[4]

Among the techniques to visualize protein–protein interactions, nuclear magnetic resonance (NMR) spectroscopy is particularly suited to weak ones. Protein–protein complexes with K_D values up to a few millimolar can be determined by using solution NMR spectroscopy on the basis of intermolecular nuclear Overhauser effect (NOE).[4–5] But the questions are whether even weaker interactions—with K_D values in the tens of millimolar—exist and can be detected and characterized, and whether these ultra-weak interactions are functionally relevant. To address these questions, however, calls for more sensitive biophysical and NMR techniques.

Phosphorylation is an important cell signaling mechanism that employs a phosphoryl group as the token of signal.[6] Phosphotransferase system (PTS) is a two-component signaling network in bacteria, responsible for sensing and using a certain nutrient.[7] In the PTS, enzyme I (EI) is first autophosphorylated,[8] and then transfers the phosphoryl group to enzyme IIA-Glucose ($EIIA^{Glc}$) via enzyme histidine phosphorcarrier (HPr).[9] As an alternative pathway, we found that, $EIIA^{Glc}$ can be phosphorylated by EI in the absence of HPr, at the same active-site residue H90 based on these evidences.

The NMR spectra of the phosphorylated $EIIA^{Glc}$ (p-$EIIA^{Glc}$) are identical either in the presence or absence of HPr (Figure 1a and Figure S1 in the Supporting Information). From the increase in peak intensities for *p*-$EIIA^{Glc}$ and the simultaneous decrease in peak intensities for the unphosphorylated $EIIA^{Glc}$, we were able to monitor the progress of $EIIA^{Glc}$ phosphorylation (Figure 1b). Addition of an HPr active-site[10] mutant, HPr-H15 A, obstructs the direct phosphorylation of $EIIA^{Glc}$ by EI, in a dose-dependent manner (Figure 1c), as the mutant competes for the same interfaces and forms non-productive complexes. The direct phosphoryl transfer from EI to $EIIA^{Glc}$ was also confirmed in vivo. With the gene-encoding HPr protein, *ptsH*, knocked out from the *E. coli* genome, the resulting Δ*ptsH* strain was still able to grow on the minimum medium and consume glucose, albeit at a slower rate (Figure 1d). With the HPr-H15A mutant gene

[*] P. Huang,[+] Prof. W.-P. Zhang[+]
Department of Pharmacology and Institute of Neuroscience
Zhejiang University School of Medicine
Yu-Hang-Tang Road, Hangzhou, Zhejiang 310028 (China)
E-mail: weiping601@zju.edu.cn
Q. Xing,[+] J. Yang, J.-Q. Sun, Dr. Z. Gong, Dr. X. Dong, Dr. D.-C. Guo, S.-M. Chen, Y.-H. Yang, Y. Wang, Prof. M.-H. Yang, Dr. M. Yi, Prof. Y.-M. Ding, Prof. M.-L. Liu, Prof. C. Tang
CAS Key Laboratory of Magnetic Resonance in Biological Systems
Wuhan Center for Magnetic Resonance
State Key Laboratory of Magnetic Resonance and Atomic Molecular Physics, Wuhan Institute of Physics and Mathematics of the Chinese Academy of Sciences
Xiao-Hong Shan, Wuhan, Hubei 430071 (China)
E-mail: tanglab@wipm.ac.cn
Homepage: http://tanglab.wipm.ac.cn
[+] These authors contributed equally to this work.

[**] We thank the Chinese Ministry of Science and Technology (grant number 2013CB910200) and the National Natural Sciences Foundation of China (grant numbers 31225007 and 31170728) for support. C.T. was supported in part by an International Early Career Scientist grant from the Howard Hughes Medical Institute. The coordinates for the EIN-$EIIA^{Glc}$ complex at 2% occupancy together with experimental restraints are deposited in the PDB with the accession code 2MP0.

Supporting information for this article is available on the WWW under http://dx.doi.org/10.1002/anie.201405976.

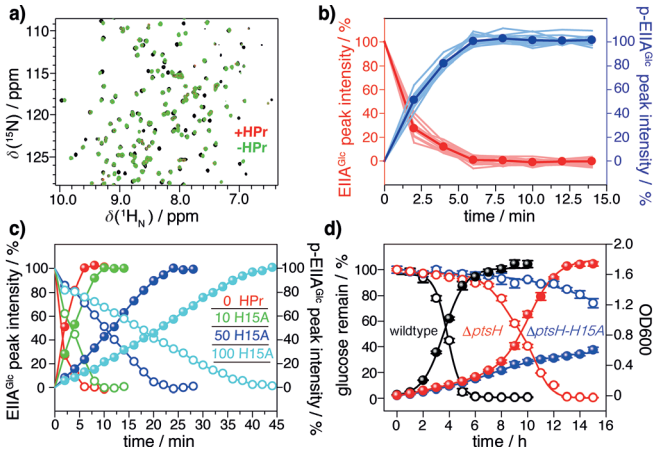

Figure 1. Phosphorylation of EIIA^{Glc} by enzyme EI. a) Overlay of 2D ^{1}H–^{15}N correlation spectra for the unphosphorylated EIIA^{Glc} (black) and phosphorylated EIIA^{Glc} either through HPr (red) or by EI directly (green). Note that the green spectrum is right on top of the red one. b) Time course of EIIA^{Glc} phosphorylation. Each light trace represents the change in relative peak intensity for a residue during phosphorylation. The averaged ratios are shown as filled circles and are connected by a solid line. c) EIIA^{Glc} phosphorylation (300 μM) by a catalytic amount of EI (0.3 μM) is obstructed by the increasing amount of HPr active-site mutant HPr-H15A (0, 3, 15, 30 μM for red, green, blue, and cyan lines, respectively). d) Growth curves (measured by OD600) and glucose consumption are compared between the wild-type, Δ*ptsH* and Δ*ptsH*-H15A strains. The Δ*ptsH* strain is obtained by knocking out the gene encoding HPr protein, *ptsH*, from the *E. coli* genome; the Δ*ptsH*-H15A strain is obtained by knocking back the HPr-H15A mutant gene.

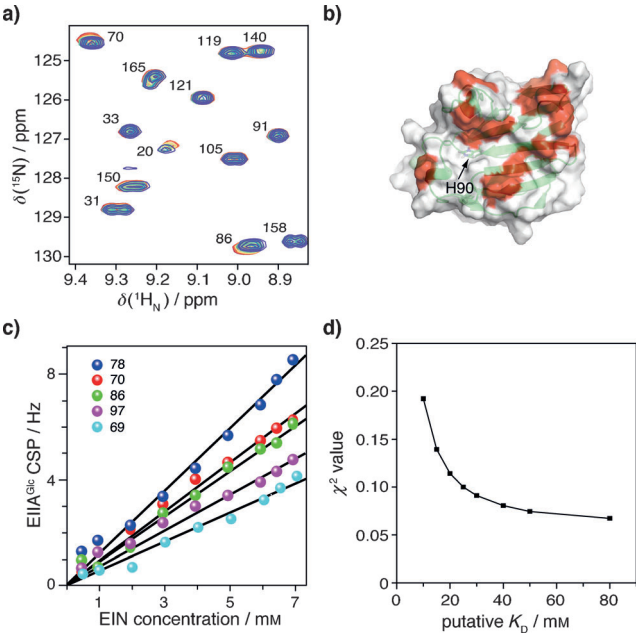

Figure 2. NMR titration of EIIA^{Glc} with EIN. a) Overlay of a region of 2D ^{1}H–^{15}N correlation spectra of EIIA^{Glc} titrated with EIN up to 7 mM. The spectral resolutions in $^{1}H_N$ and ^{15}N dimensions are 4.695 Hz/point and 7.128 Hz/point, respectively. b) Residues with chemical shift perturbations (CSPs) > 3 Hz are mapped onto the surface of EIIA^{Glc}. c) EIIA^{Glc} CSPs are plotted against the concentrations of EIN. d) EIIA^{Glc} CSPs are fitted to theoretical binding isotherms with putative K_D values. The residual χ^2 values from the fitting are plotted against the K_D.

knocked back in, the Δ*ptsH*-H15A strain was found to grow more slowly with slower glucose consumption than the Δ*ptsH* strain (Figure 1d). Taken together, enzyme EI phosphorylates EIIA^{Glc} directly. In doing so, enzyme EI, especially its N-terminal domain (EIN) where the active-site residue H189 is located,[8] has to directly interact with EIIA^{Glc}.

The binding affinity between EI and EIIA^{Glc}, however, turned out to be extremely weak. We performed NMR titration with the unlabeled EIN, up to 7 mM, into the ^{15}N-labeled EIIA^{Glc}. The resulted chemical shift perturbations (CSPs) for EIIA^{Glc} are smaller than 9 Hz or about 0.01 ppm on an 800 MHz NMR spectrometer (Figure 2a). Titration of the full-length EI, up to 4 mM, into EIIA^{Glc} gives even smaller CSPs for EIIA^{Glc} (Figure S2). Though most of the perturbed residues form a somewhat contiguous surface and can be mapped to the vicinity of EIIA^{Glc} active-site residue H90 (Figure 2b), plotting EIIA^{Glc} CSPs against EIN protein concentration yields almost straight lines (Figure 2c). A plausible fit for the CSPs can only be obtained with a K_D value larger than 20 mM, as the residual χ^2 value begins to level off (Figure 2d and Figure S3). Inverse titration of unlabeled EIIA^{Glc} into U-[^{2}H,^{15}N]-labeled EIN affords even smaller CSPs (Figure S4). The small CSPs result from the extremely low occupancy of the EIN-EIIA^{Glc} complex at the concentrations permitted by protein solubility. As the standard NMR approach requires a significant population of the protein in the complexed form,[4] it would not be feasible to characterize the structure of the EIN-EIIA^{Glc} complex based on intermolecular NOEs.

Thus we resorted to paramagnetic NMR spectroscopy.[11] We were only able to obtain intermolecular restraints using a Gd^{3+}-based paramagnetic probe; Gd^{3+}-EDTA-benzyl-acetate (Figure S5) was conjugated at an engineered cysteine in either EIN or EIIA^{Glc}, and the paramagnetic relaxation enhancement (PRE) rates were assessed for the ^{15}N-labeled partner protein. Gd^{3+} is a lanthanide ion with a large spin quantum number ($S = 7/2$) and long electron relaxation time ($\tau_e \approx 10$ ns).[12] At a given electron–proton distance, Gd^{3+} causes the PRE effect twice as large as transition metal Mn^{2+} and ten times as large as nitroxide radical. Despite of the more favorable relaxation property of Gd^{3+}, intermolecular PREs for some of the conjugation sites (Q87C, S113C, and E117C on EIN) are still smaller than 5 s^{-1}. The largest intermolecular PREs were afforded for EIIA^{Glc} with the probe conjugated at the EIN E63C site, and for EIN with the probe conjugated at the EIIA^{Glc} E43C site (Figure 3). Even for these two sites, no residue was completely broadened out or has a PRE value > 80 s^{-1}.

To determine the complex structure, we performed rigid-body simulated annealing, by refining against the intermolecular PRE restraints for EIN E63C, EIN E117C, and EIIA^{Glc} E43C sites. The occupancy of the complex was varied from 0.1 to 5%. The best agreement between the observed and back-calculated Gd^{3+} PREs was achieved with the complex formed at 2–5% of the time, while occupancy of 1% or less resulted in large van der Waals repulsive energy and large PRE Q-factor (Figure 4a). At the protein concentrations employed for the PRE experiments, a 2% occupancy

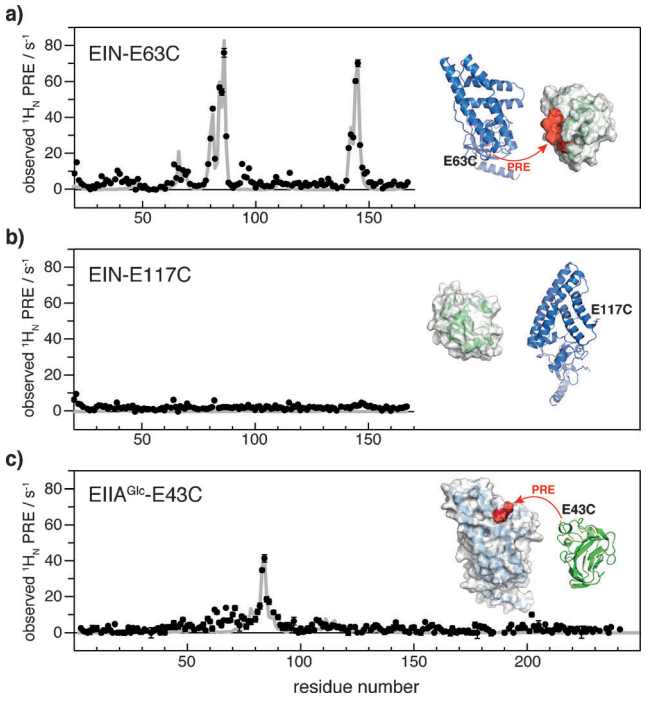

Figure 3. Intermolecular PREs between EIN and EIIA^{Glc}. Using a Gd^{3+}-based paramagnetic probe, the PRE values were measured for a) EIIA^{Glc} at EIN E63C, b) for EIIA^{Glc} at E117C sites, and c) for EIN at EIIA^{Glc} E43C site. Observed PREs are shown as black dots, error bar representing 1 standard deviation. The back-calculated PREs are shown as grey lines. Insets show the structures of individual proteins, with the cysteine conjugation sites and residues with large PREs ($\Gamma_2 > 20\ s^{-1}$) illustrated.

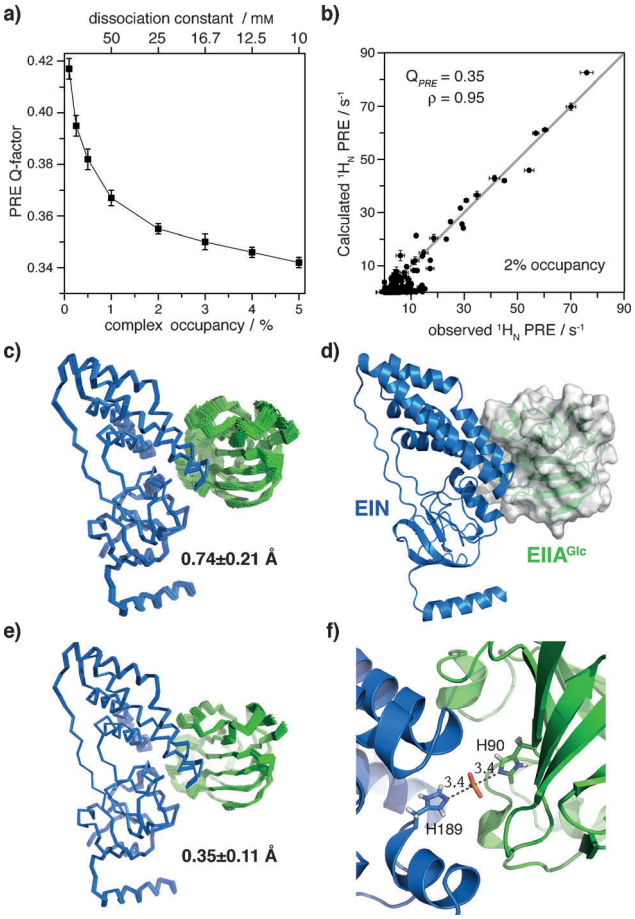

Figure 4. Structure of the EIN-EIIA^{Glc} complex. a) Overall PRE Q-factor as a function of the population of the complex. With the concentration of both proteins at 0.5 mM, a 2% occupancy corresponds to a K_D value of 25 mM (top scale). b) The PRE Q-factor and correlation coefficient ρ between observed and calculated PREs at 2% occupancy of the complex. The diagonal line indicates a perfect correlation, simply to guide the eyes. c,e) Ribbon representation for the EIN-EIIA^{Glc} complex, with backbone rms deviations indicated. Covalent geometrical restraints were incorporated when calculating the structure shown in panel (e). The ensemble was selected based on overall energy, PRE Q-factor, and deviation from the mean structure. d) Cartoon and surface representation for the complex. f) Close-up view of the complex showing the phosphorylation transition state. The distances to the phosphoryl group being transferred are labeled.

of the complex corresponds to a K_D value of about 25 mM for the EIN-EIIA^{Glc} interaction, which is within the range deduced from the CSP fitting (Figure 2d).

At 2% occupancy for the EIN-EIIA^{Glc} complex, the overall PRE Q-factor is 0.35 and the correlation coefficient is 0.95 between the observed and calculated PREs (Figure 4b). The complex structure converges to a well-defined conformation, affording root-mean-square (rms) differences of 0.74 ± 0.21 Å for the backbone and 0.99 ± 0.17 Å for all heavy atoms (Figure 4c and d). When enforcing a covalent geometry for the phosphorylation transition state, the structural convergence can be improved to 0.35 ± 0.11 Å for the backbone and 0.69 ± 0.07 Å for all heavy atoms (Figure 4e and Table S1), while the PRE Q-factor remains the same. In the transition-state complex, the distances from the phosphorus atom in the phosphoryl group to the Nε2 atoms of the active site histidines in EIN and EIIA^{Glc} are both 3.4 Å (Figure 4f), which is characteristic of a dissociative transition state for the phosphorylation reaction.[5b,13] As such, the complex structure explains how a phosphoryl group can be transferred between EI and EIIA^{Glc}. Though a well-defined complex structure is required to enable phosphoryl transfer, encounter complexes between EI and EIIA^{Glc} at even lower occupancies may exist.[14] Indeed, EIIA^{Glc} residues 38-40 and 94-97 at EIN-E63C site and EIN residues 62-71 at EIIA^{Glc}-E43C site experience PREs $> 5\ s^{-1}$ but are not fully accounted for (Figure 3).

EIN and EIIA^{Glc} are highly complementary in shape in their complex, as EIIA^{Glc} saddles over a helix of EIN (Figure 4d) and affords a total buried solvent accessible surface area of 1517 ± 128 Å^2. Over a dozen hydrophobic aliphatic and aromatic residues, including I72, L79, L115, L118, L123, and V130 in EIN and V39, V40, F41, I45, V46, F71, F88, V96 in EIIA^{Glc}, are located near the active-site residues, which would favor the formation of the complex. On the other hand, the interfaces are highly negatively charged on both EIN and EIIA^{Glc} (Figure 5a and Figure S6), which can account for the ultra-weak affinity between the two proteins.

To assess the role of charged residues at the buried interfaces, we designed a charge reversal mutant, by mutating EIIA^{Glc} residue E86 to a lysine. Titration of this E86K mutant

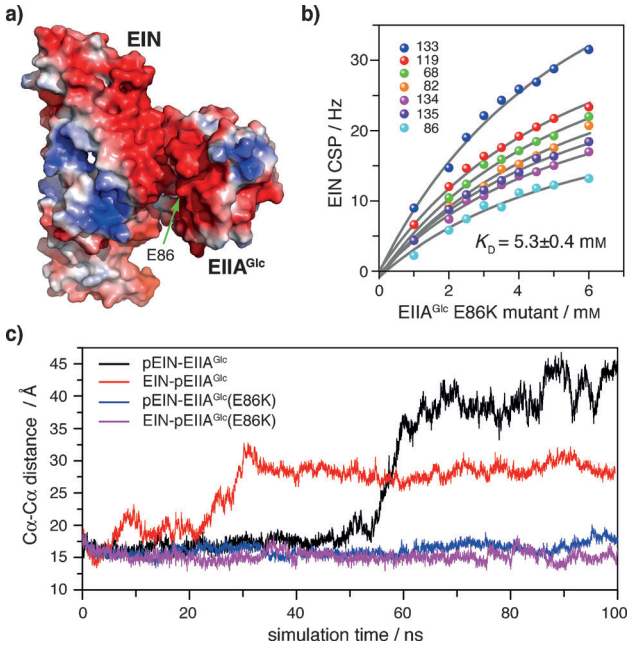

Figure 5. Physical basis for the fleeting interaction between EI and EIIA^{Glc}. a) Solvent accessible surface of EIN-EIIA^{Glc} complex colored by electrostatic potential, on a scale from −3 kT (red) to 3 kT (blue). The mutated residue in EIIA^{Glc} is denoted with a green arrow. b) Titration of EIN with EIIA^{Glc} E86K mutant protein affords CSPs that can be globally fitted to a binding isotherm. c) The distances between the Cα atoms of H189 in EIN and H90 in EIIA^{Glc} (either wild-type or E86 K mutant) during accelerated MD simulations for the fleeting complex, with the phosphoryl group attached to either EIN or EIIA^{Glc}.

of EIIA^{Glc} to EIN perturbed the same set of residues on the EIN surface as the titration with the wild-type EIIA^{Glc}, yet the magnitude of the CSPs are much larger (Figure 5b). Among the perturbed residues, residue E68 in EIN displays a 20 Hz CSP, compared to a mere 4 Hz when titrated with the wild-type EIIA^{Glc} (Figure S4). Importantly, the EIN CSPs can now be fitted to a global binding isotherm, affording a K_D value of 5.3 ± 0.4 mM (Figure 5b).

To elucidate the dynamic feature of the EIN–EIIA^{Glc} complex, we performed accelerated molecular dynamics (aMD) simulations.[15] During the phosphorylation signaling, a phosphoryl group can be either attached to EIN residue H189 or EIIA^{Glc} residue H90. The free energies calculated for these two intermediate complexes, pEIN–EIIA^{Glc} and EIN–pEIIA^{Glc}, are −9.5 and −4.3 kcal mol^{-1}, respectively. Thus, the complex is more stable with EIN phosphorylated than with EIIA^{Glc} phosphorylated. Accordingly, during the aMD simulations, the EIN–pEIIA^{Glc} complex dissociates more readily than the pEIN–EIIA^{Glc} complex does (Figure 5c). As such, the relative stabilities of these two intermediate complexes dictate that the phosphoryl signal flows from EI to EIIA^{Glc}.

Dissociation of protein–protein complexes are usually recapitulated with steered MD simulations, as the lifetime of most complexes is too long to be simulated with unbiased MD simulations.[16] The fact that the EIN–EIIA^{Glc} dissociation can be visualized with the aMD indicates that the complex is short-lived, likely on the timescale from micro- to milliseconds. Hence we term such interaction a fleeting interaction. Upon introducing an E86 K mutation to EIIA^{Glc}, the EIN–EIIA^{Glc} complex remains associated during the aMD simulations, no matter to which protein the phosphoryl group is attached (Figure 5c). As such, the charge-reversal mutation not only enhances the binding affinity, but also prolongs the lifetime of the otherwise fleeting complex.

With a K_D value of about 25 mM, the complex between EI and EIIA^{Glc} is almost an order of magnitude weaker than all known protein–protein complexes with high-resolution structures available.[4,5] So what are the advantages for such weak fleeting interaction in phosphorylation signaling? The general notion for cell signaling has been that, when stimulated, the expression level of a protein is either up-regulated or down-regulated, leading to a modulation of the corresponding signal. Here we constructed a mathematical model for an open phosphoryl transfer process within a large two-component system, and our calculation shows that higher protein concentration does lead to an amplification of phosphoryl signal (Figure 6a)—up to a 100-fold change in phosphoryl flux for every 10-fold change of protein concentration. However, the full capacity of such modulation can only be achieved when the affinity between the two interacting proteins, as measured by the K_D value, is comparable to or larger than the protein concentration (Figure 6b). If the K_D value is smaller than the protein concentration, the modulation of phosphoryl flux is relatively insensitive to the change in protein concentration.

The relationship between phosphoryl flux and K_D can also be grasped from the definition of the K_D, that is, the ratio between kinetic dissociation rate k_{off} and association rate k_{on}. A weak protein–protein interaction corresponds to a large kinetic dissociation rate k_{off} at a certain association rate k_{on}. Dissociation is intrinsic to a protein complex, whereas association can be promoted by high concentration.[17] Increasing evidences have shown that protein is unevenly distributed in cell and the local effective concentration can be well above 1 mM,[18] owing to a number of factors, such as

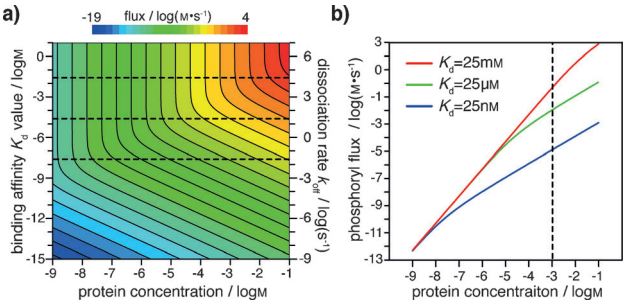

Figure 6. Phosphoryl flux as a function of the protein concentration and binding affinity K_D. a) Heat map of the phosphoryl flux from protein A to protein B at a kinetic association rate k_{on} of 10^6 M^{-1} s^{-1}. The corresponding kinetic dissociation rate k_{off} is labeled on the right, which is equal to $k_{on}K_D$. The dashed lines denote the K_D values of 25 nM, 25 μM and 25 mM, respectively. b) At these three K_D values, the phosphoryl flux as a function of protein concentration is plotted. When the protein concentration is 1 mM (denoted by a dashed line), the red flux is larger than 43 fold of the green flux, and larger than 37000 fold of the blue flux.

macromolecular crowding,[19] being part of a multi-protein complex, association with a common scaffold protein,[20] membrane anchoring,[21] and covalent linkage.[22] Thus, too strong binding at high concentration would trap the signaling proteins in a bound state, making the release of the phosphorylated product the rate-limiting step.[23]

To summarize, we have shown that phosphoryl signaling can be accomplished by an ultra-weak fleeting interaction between two bacterial enzymes. We introduced a Gd^{3+}-based probe in PRE NMR spectroscopy for the first time, and we determined the atomic resolution structure of the ultra-weak complex that is otherwise too fleeting to visualize. Though marginally stable, such a fleeting interaction would enable effective modulation of cell signal upon the changes in protein concentration. Given the millimolar effective concentrations of many proteins in cell, fleeting interactions can be prevalent among signaling proteins, which awaits further exploration.

Received: June 6, 2014
Published online: August 11, 2014

Keywords: NMR spectroscopy · paramagnetic relaxation enhancement · proteins · protein–protein interactions · signal transduction

[1] L. J. Jensen, M. Kuhn, M. Stark, S. Chaffron, C. Creevey, J. Muller, T. Doerks, P. Julien, A. Roth, M. Simonovic, P. Bork, C. von Mering, *Nucleic Acids Res.* **2009**, *37*, D412 – 416.
[2] J. R. Perkins, I. Diboun, B. H. Dessailly, J. G. Lees, C. Orengo, *Structure* **2010**, *18*, 1233 – 1243.
[3] a) I. M. Nooren, J. M. Thornton, *J. Mol. Biol.* **2003**, *325*, 991 – 1018; b) H. Hwang, T. Vreven, J. Janin, Z. Weng, *Proteins Struct. Funct. Bioinf.* **2010**, *78*, 3111 – 3114; c) P. L. Kastritis, I. H. Moal, H. Hwang, Z. Weng, P. A. Bates, A. M. Bonvin, J. Janin, *Protein Sci.* **2011**, *20*, 482 – 491.
[4] O. Vinogradova, J. Qin, *Top. Curr. Chem.* **2012**, *326*, 35 – 45.
[5] a) R. Wang, X. Fang, Y. Lu, S. Wang, *J. Med. Chem.* **2004**, *47*, 2977 – 2980; b) Y. S. Jung, M. Cai, G. M. Clore, *J. Biol. Chem.* **2012**, *287*, 23819 – 23829; c) M. A. Hass, M. Ubbink, *Curr. Opin. Struct. Biol.* **2014**, *24*, 45 – 53.
[6] T. Hunter, *Philos. Trans. R. Soc. London Ser. B* **2012**, *367*, 2513 – 2516.
[7] J. Deutscher, C. Francke, P. W. Postma, *Microbiol. Mol. Biol. Rev.* **2006**, *70*, 939 – 1031.
[8] V. Venditti, G. M. Clore, *J. Biol. Chem.* **2012**, *287*, 26989 – 26998.
[9] P. W. Postma, J. W. Lengeler, G. R. Jacobson, *Microbiol. Rev.* **1993**, *57*, 543 – 594.
[10] D. S. Garrett, Y. J. Seok, A. Peterkofsky, A. M. Gronenborn, G. M. Clore, *Nat. Struct. Biol.* **1999**, *6*, 166 – 173.
[11] G. M. Clore, J. Iwahara, *Chem. Rev.* **2009**, *109*, 4108 – 4139.
[12] I. Bertini, C. Luchinat, S. Aime, *Coord. Chem. Rev.* **1996**, *150*, 77 – 110.
[13] G. Wang, J. M. Louis, M. Sondej, Y. J. Seok, A. Peterkofsky, G. M. Clore, *EMBO J.* **2000**, *19*, 5635 – 5649.
[14] a) C. Tang, J. Iwahara, G. M. Clore, *Nature* **2006**, *444*, 383 – 386; b) A. N. Volkov, J. A. Worrall, E. Holtzmann, M. Ubbink, *Proc. Natl. Acad. Sci. USA* **2006**, *103*, 18945 – 18950; c) Y. Hiruma, M. A. Hass, Y. Kikui, W. M. Liu, B. Olmez, S. P. Skinner, A. Blok, A. Kloosterman, H. Koteishi, F. Lohr, H. Schwalbe, M. Nojiri, M. Ubbink, *J. Mol. Biol.* **2013**, *425*, 4353 – 4365.
[15] D. Hamelberg, J. Mongan, J. A. McCammon, *J. Chem. Phys.* **2004**, *120*, 11919 – 11929.
[16] R. O. Dror, R. M. Dirks, J. P. Grossman, H. Xu, D. E. Shaw, *Annu. Rev. Biophys.* **2012**, *41*, 429 – 452.
[17] X. Pang, S. Qin, H. X. Zhou, *Biophys. J.* **2011**, *101*, 1175 – 1183.
[18] J. A. Ubersax, J. E. Ferrell, Jr., *Nat. Rev. Mol. Cell Biol.* **2007**, *8*, 530 – 541.
[19] a) H. X. Zhou, G. Rivas, A. P. Minton, *Annu. Rev. Biophys.* **2008**, *37*, 375 – 397; b) B. Akabayov, S. R. Akabayov, S. J. Lee, G. Wagner, C. C. Richardson, *Nat. Commun.* **2013**, *4*, 1615.
[20] T. J. Gibson, *Trends Biochem. Sci.* **2009**, *34*, 471 – 482.
[21] X. Shi, Y. Bi, W. Yang, X. Guo, Y. Jiang, C. Wan, L. Li, Y. Bai, J. Guo, Y. Wang, X. Chen, B. Wu, H. Sun, W. Liu, J. Wang, C. Xu, *Nature* **2013**, *493*, 111 – 115.
[22] J. Y. Suh, J. Iwahara, G. M. Clore, *Proc. Natl. Acad. Sci. USA* **2007**, *104*, 3153 – 3158.
[23] S. A. Lieser, B. E. Aubol, L. Wong, P. A. Jennings, J. A. Adams, *Biochim. Biophys. Acta Proteins Proteomics* **2005**, *1754*, 191 – 199.

Angewandte Chemie
Eine Zeitschrift der Gesellschaft Deutscher Chemiker

Supporting Information

69451 Weinheim, Germany

Visualizing an Ultra-Weak Protein–Protein Interaction in Phosphorylation Signaling**

Qiong Xing, Peng Huang, Ju Yang, Jian-Qiang Sun, Zhou Gong, Xu Dong, Da-Chuan Guo, Shao-Min Chen, Yu-Hong Yang, Yan Wang, Ming-Hui Yang, Ming Yi, Yi-Ming Ding, Mai-Li Liu, Wei-Ping Zhang, and Chun Tang**

anie_201405976_sm_miscellaneous_information.pdf

Experimental Section

Sample preparation. Genes encoding PTS proteins including the full-length enzyme I, EIN (N-terminal domain of enzyme including residues 1-249), HPr and enzyme IIA^{Glc} ($EIIA^{Glc}$) were PCR amplified from *E. coli* cells and were cloned into a pET11a vector. Cysteine single-point mutants of EIN E63C, EIN E117C and $EIIA^{Glc}$ E43C were introduced, one at a time, using QuikChange (Stratagene) and were confirmed by DNA sequencing. HPr-H15A mutant carrying a C-terminal hexahistidine tag and $EIIA^{Glc}$ E86K mutant were constructed in the same fashion. Proteins were expressed in BL21 (DE3) star cells at 37 ºC and were induced with 0.5 mM IPTG for 4-8 hours (4 hours in LB and 8 hours in minimal medium). LB medium or M9-minimum medium was used for making unlabeled protein or isotope-enriched protein. In the latter, U-$^{15}NH_4Cl$ was supplied as the sole nitrogen source for bacterial growth. Wildtype U-[^{2}H, ^{15}N]-labeled EIN protein was expressed in D_2O medium containing perdeuterated glucose, spiked with 1g/L IsoGrow (Isotec). After cell lysis using a microfluidic device (EmulsiFlex-C3 by Avestin), proteins were first purified with a DEAE ion exchange fast-flow column (HPr-H15A was first purified with a HisTrap Ni-NTA affinity column), followed by S100 size exclusion column, and then with Mono-Q ion exchange column (GE Healthcare). For the last purification step, proteins were eluted off a Mono-Q column on a 100mL 10-500 mM NaCl gradient in pH 7.4 Tris•HCl buffer, with HPr eluted off a Mono-Q at ~5 mS/cm, EIN at ~30 mS/cm, and $EIIA^{Glc}$ at ~19 mS/cm. Cysteine mutants elutes off slightly earlier than the wildtype proteins due to the loss of a negative charge. Proteins were concentrated and buffer-exchanged in Amicon filters (Millipore), and were confirmed by LC-ESI-TOF mass spectrometry (Bruker Daltonics).

NMR titration. Protein samples were prepared in a 10mM pH 7.2 Tris•HCl buffer with 10% D_2O and 100 mM NaCl. ^{1}H-^{15}N HSQC spectra were collected at 313 K on a Bruker Avance III 800 MHz spectrometer equipped with a cryogenic probe. The concentration of ^{15}N-labeled protein was kept at 1mM, and the titrant concentration of the unlabeled protein was gradually increased to 7 mM (up to 6 mM for $EIIA^{Glc}$ E86K mutant and up to 4 mM for full-length EI). The differences in NMR chemical shifts were recorded as the geometrical averages for the values of backbone amide proton and nitrogen. The spectral resolutions in ^{1}H and ^{15}N dimensions are 4.695 Hz/point and 7.128 Hz/point, respectively.

Enzyme kinetics monitored by NMR. To initiate the phosphorylation reaction and to ensure full activity of the enzymes, the NMR buffer comprised 5 mM $MgCl_2$, 1 mM DTT, 1 mM EDTA and 10 mM PEP (Alfa Aesar), 10% D_2O in 50 mM pH 7.4 Tris buffer. 0.3 μM of EI was added to 300 μM ^{15}N-labeled $EIIA^{Glc}$ (as a negative control, no EI was added and $EIIA^{Glc}$ remained unphosphorylated); 0, 3, 15 or 30 μM of His-tagged HPr-H15A mutant proteins (0×, 10×, 50× and 100× fold excess of EI, respectively) was added into the reactions. A series of 2D ^{1}H-^{15}N correlation spectra were collected at 310 K on a Bruker 800MHz instrument for ^{15}N-labeled $EIIA^{Glc}$ using a SOFAST pulse scheme,[1] while monitoring the progress of phosphorylation.

Cell-based experiments. Homologous recombination was carried out between *ptsH* gene (the gene encoding HPr protein) and a PCR-generated Kan^R-pheS cassette, to knock out the gene from the *E. coli* chromosome using a phage λ-Red recombination system.[2] The resulted *E.coli* strain, Δ*ptsH*, was verified with PCR, as the wildtype HPr band was absent on the DNA gel and a new band at 2.4 kb appeared corresponding to the substituted Kan^R-pheS cassette. A second round of homologous recombination was performed between Kan^R-pheS cassette on the chromosome of Δ*ptsH* and *ptsH* gene with an H15A mutation. The resulting *E.coli* strain, Δ*ptsH*-H15A, was verified by PCR and by DNA sequencing.

To measure the growth rate of wildtype DH10B, Δ*ptsH* and Δ*ptsH*-H15A, cells were grown on a modified M9 minimum medium containing 2 g/L glucose, 100 mg/L thiamine, 2 mM $MgSO_4$, 0.1 mM $CaCl_2$, and 20 amino acids 40 mg/L each as described.[3] A single colony was inoculated into 5 mL LB medium and was grown overnight at 37 °C before transferring to minimal medium — cells from LB were washed twice and diluted by 1:100 into M9 minimal medium. Optical density readings at 600 nm (OD600) were taken every 30 min for plotting growth curves. Concentrations of remaining glucose were also measured at the same time points by following the manufacturer's instruction (BioSino Biotechnology). All cell cultures were done in triplicate, and readings on 200 μL from the culture were taken in a 96-well plate in Multiskan Ascent photometer (Thermo Scientific).

PRE experiment. A single-point cysteine mutant protein was reacted with (S)-1-(p-bromo-acetamido benzyl) ethylenediamine-tetraacetate (abbreviated as BABE,[4] from Toronto Research Chemicals), one site at a time. For conjugation of Gd^{3+}-based probe, BABE was first mixed with $GdCl_3$•$6H_2O$ (Sigma Aldrich) at 1:2 molar ratio in a pH 6.0 sodium acetate buffer. After removing the reducing agent from the buffer by desalting,

the cysteine mutant protein was allowed to react with BABE and $GdCl_3 \bullet 6H_2O$ at a molar ratio of 1:2.5:5 at room temperature overnight. Unreacted probe and metal were removed by desalting. Conjugated and chelated protein was further purified on Mono-Q ion exchange column. 0.5 mM ^{15}N labeled protein was mixed equimolar with paramagnetically tagged natural isotope abundance protein. Protein NMR samples were prepared in 10 mM pH 7.2 Tris•HCl with 10% D_2O and 100 mM NaCl and data were acquired at 313 K on a Bruker 600 MHz spectrometer equipped with a cryogenic probe. For the TROSY scheme measured for the deuterated EIN, the interleaved delay block was placed after the last INEPT transfer and before acquisition. □□ relaxation rates were measured for backbone amide with the standard pulse sequence,[5] using 9 time points with a total delay of 32 ms. An inversion recovery sequence was used to measured amide proton R_1 rates. PRE Γ_1 and Γ_2 rates were calculated by subtracting diamagnetic contributions from paramagnetic values for the deuterated EIN, or by taking the ratio of two-time-point signal decay over the same delay for the ^{15}N-labeled $EIIA^{Glc}$.

Structure calculation. The pseudopotential energy for the cysteine-derivatized and Gd^{3+}-chelated paramagnetic probe was calculated with fine integral grid using Gaussian-09 software package (Gaussian). At B3LYP/6-31G* level, dihedral angles ζ1 and ζ2 were allowed to vary, from 0 to 360º in 10º steps, with the rest of the probe fixed. The (ζ1, ζ2) heat map was plotted in Software Origin 8.1. Two lowest-energy configurations of the probe, with (ζ1, ζ2) of (60º, 180º) and (240º, 180º) were identified and were used in the following refinement of EIN-$EIIA^{Glc}$ complex structure.

Refinement against experimental restraints was carried out using Xplor-NIH.[6] A six-conformer representation (three conformers for each ζ1/ζ2 configuration) of the paramagnetic probe was employed for each conjugation site (EIN E63C, EIN E117C and $EIIA^{Glc}$-E43C), allowing the χ1, χ2, χ3, χ4 angles to freely rotate, thus to recapitulate the flexibility of the paramagnetic probe.[5] The starting structure of EIN was taken from PDB structure 1ZYM[7] chain A, and the structure of $EIIA^{Glc}$ was taken from 1F3Z[8] chain A. Rigid-body refinement was performed with a target function comprising the intermolecular PRE restraints for all three tagging sites, a van der Waals repulsive term and a weak radius-of-gyration restraint[9] to the putative interfacial residues mapped by NMR chemical shift perturbation (including residues 59, 68-69, 82 and 118 in EIN and residues 40-46, 69-70, 78, 84-87, 97, 143-149 in $EIIA^{Glc}$). While keeping EIN fixed, $EIIA^{Glc}$ was first treated as a rigid body and was allowed to rotate and translate. With its *f* orbital half-occupied, Gd^{3+} has a symmetric *g*-tensor and a spin quantum number *s* of 7/2.

An apparent PRE correlation time (τ_c = 6.7 ns) was estimated from the rotational correlation time of the complex based on hydrodynamics calculation (τ_r = 20 ns) and the electron relaxation time of Gd^{3+} (τ_e = 10 ns[10]). The population of the complex was varied from 0.1% to 5%, which was used as a scaling factor for the back-calculated PREs. After the initial pose for the EIN-EIIA^{Glc} complex was identified, side chains of interfacial residues were allowed to rotate,[11] and knowledge-based side chain conformational restraints[12] were supplemented to improve packing at the interface. The agreement between observed and calculated PRE rates are assessed by the PRE Q-factor, which is defined as

$$Q_{PRE} = \left\{ \sum_i \left[\Gamma_2^{obs}(i) - \left\langle \Gamma_2^{calc}(i) \right\rangle \right]^2 / \sum_i \Gamma_2^{obs}(i)^2 \right\}^{1/2},$$

in which $\langle \Gamma_2^{Calc} \rangle$ is the PRE value calculated for each residue averaged over all conformers. The overall PRE Q-factor is 0.35 (0.27, 0.96, 0.56 for EIN-E63C, EIN-E117C and EIIA^{Glc}-E43C, respectively), and overall correlation coefficient is 0.95 (0.97, -0.01, 0.85 for EIN-E63C, EIN-E117C and EIIA^{Glc}-E43C, respectively). At a given population *p* of the complex, the dissociation constant K_d value can be calculated using the following equation,

$$K_D = \frac{c(1-p)^2}{p} \approx c/p$$

in which *p* is between 0.001 and 0.05 while *c* is the experimental protein concentration at 0.5 mM. The solvent accessible surface area was calculated with Xplor-NIH, with a probe radius of 1.4 Å, and was averaged over all conformers afforded. EIN His189 and EIIA^{Glc} His90 are both in Nδ1 tautomer at pH 7.2 and the Nε2 can be readily phosphorylated.[13] To model the transition state of phosphoryl transfer in a trigonal bi-pyramidal geometry, additional covalent restraints were applied to the phosphoryl group and the imidazole rings of EIN His189 and EIIA^{Glc} His90, including bond lengths, angles and improper angles.[14] Structural figures were illustrated using PyMol (The PyMOL Molecular Graphics System, Version 1.5, Schrödinger, LLC.)

Molecular dynamics (MD) simulations. Starting from the coordinates for the EIN-EIIA^{Glc} complex, a phosphoryl group was patched to either EIN His189 or EIIA^{Glc} His90, both at ε2 position,[13b,15] using the parameter set for phopsphohistidine from Homeyer et al.[16] The interaction free energy was calculated by using MMPBSA program in the AMBER 12 software package.[17]

To simulate the dissociation process of EIN-EIIA^{Glc} complex, accelerated MD (aMD) simulation[18] was performed in the AMBER 12 software package using the ff12SB force field. For each random seed, four traces of simulations were performed, for pEIN-EIIA^{Glc}, EIN-pEIIA^{Glc}, pEIN-EIIA^{Glc}(E86K) and EIN-pEIIA^{Glc}(E86K), respectively. The complex was first solvated in a cubic box containing the TIP3P water molecules, with a 5 Å padding in all directions. The time step was 2 fs and the SHAKE algorithm was used to constrain the bonds connecting hydrogen atoms. The Langevin thermostat was used to control the temperature at 300 K using a collision frequency of 1.0/ps. The long-range electrostatics was treated with the Particle Mesh Ewald (PME) method with default Ewald parameters and the van der Waals force was truncated at 10 Å with an energy shift. A 20 ns standard MD simulation was first performed, and the final conformer was fed to the aMD simulation. The aMD makes use of a modified energy potential, so that the simulated molecule can cross energy barriers more easily.[18] The boost parameters include dihedral boost and the total boost, which were obtained from the average dihedral and total potential energy in the 20 ns standard MD simulation. Accelerated, the time trace from aMD is accelerated and does not exactly reproduce protein dynamics — a 100 ns simulation may reach a millisecond in timescale.[19]

Modeling of phosphoryl flux. Here we consider an open system comprising phosphotransferases **A** and **B** as part of a large two-component system.

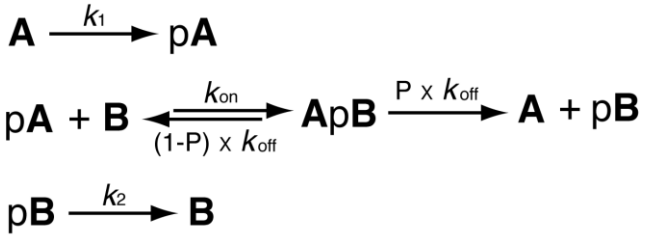

The phosphoryl group flows into the system and phosphorylates **A** at a rate constant of k_1, while the phosphoryl group flows out of the system and dephosphorylates **B** at a rate constant of k_2. The intermediate **A**p**B** may break down to either **A** and p**B**, or to p**A** and **B**. For an apparent lifetime τ for **A**p**B**, the kinetic dissociation rate k_{off} is equal to $1/\tau$ (also equal to the product of K_d and k_{on} values). The forward probability to **A** and p**B** is P, and the reverse probability to p**A** and **B** is (1-P). Based on the mass action law, a mathematical model can be obtained, with all the parameters defined in the following ordinary differential equations:

$$\frac{d[pA]}{dt} = (1-P) \times k_{off} \times [ApB] - k_{on} \times [pA] \times [B] + k_1 \times [A] \quad (1)$$

$$\frac{d[B]}{dt} = (1-P) \times k_{off} \times [ApB] - k_{on} \times [pA] \times [B] + k_2 \times [pB] \quad (2)$$

$$\frac{d[ApB]}{dt} = k_{on} \times [pA] \times [B] - k_{off} \times [ApB] \quad (3)$$

$$\frac{d[A]}{dt} = P \times k_{off} \times [ApB] - k_1 \times [A] \quad (4)$$

$$\frac{d[pB]}{dt} = P \times k_{off} \times [AB] - k_2 \times [pB] \quad (5)$$

Consistent with experimental observations and MD simulations, here we assume that the phosphoryl group flows in only one direction — **A** phosphorylates **B** while **B** does not phosphorylate **A** in the opposite direction. We assume the probability P is equal to 0.5.[20] We also assume that protein concentration ρ for both **A** and **B** is constant, and k_1, k_2 values are large enough to sustain a flux ($k_1 = k_2 = 10^8$ s^{-1}). The flux is defined as the phosphoryl group transferred through the open system per unit time in a steady state, and is equal to k_1×[A] or k_2×[pB]. We assume a typical kinetic association rate k_{on} between p**A** and **B** for 10^6 M^{-1}•s^{-1}.[21] Solving the equations using the MATLAB software with the ode23s function thus affords the relationship between flux, equilibrium dissociation K_d and protein concentration ρ.

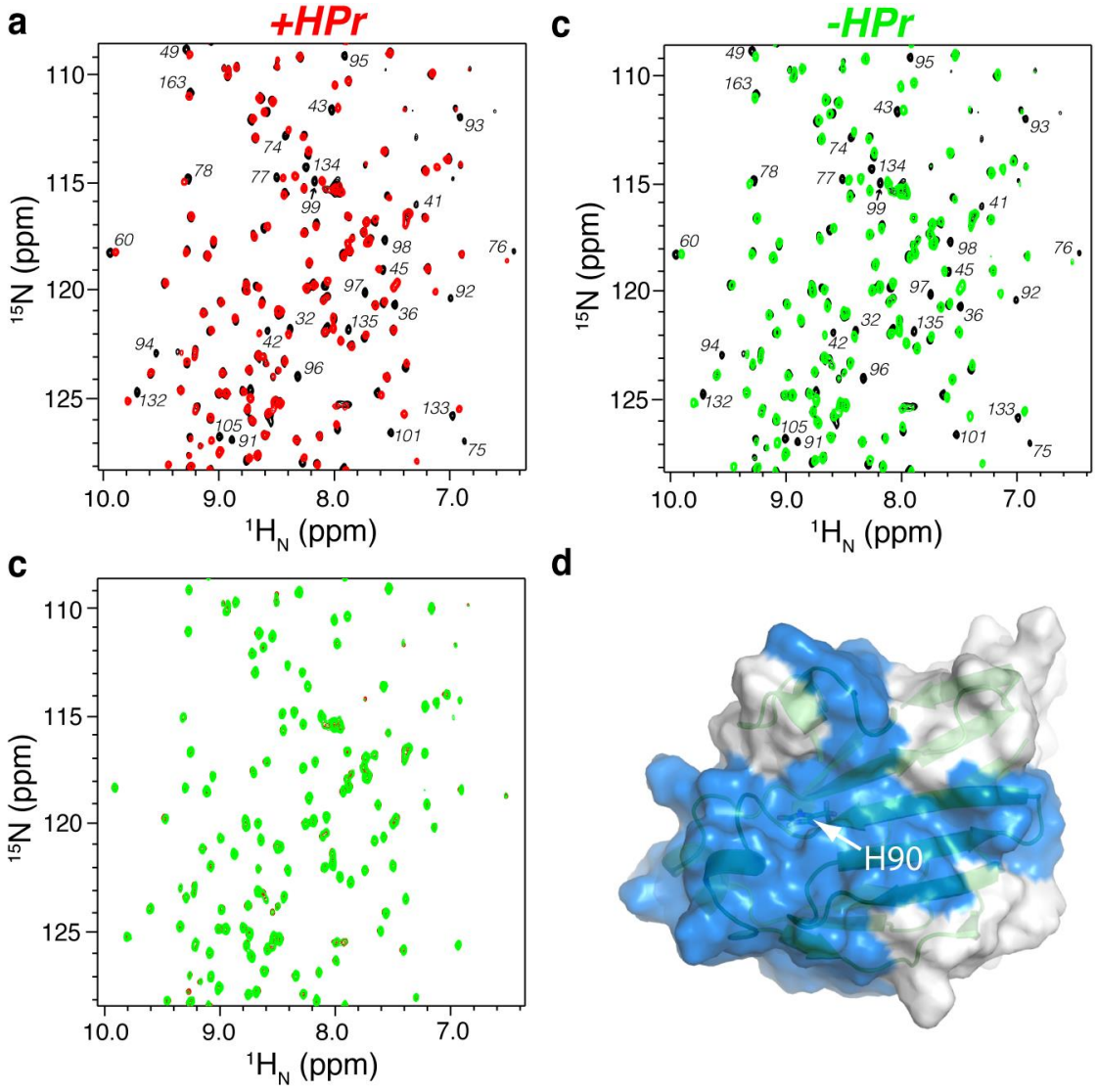

Figure S1. EIIA^{Glc} can be directly phosphorylated by EI. a) Overlay of 2D ^{1}H-^{15}N correlation spectra for the unphosphorylated EIIA^{Glc} (black) and phosphorylated EIIA^{Glc} by EI through HPr (red). b) Overlay of 2D NMR spectra for the unphosphorylated EIIA^{Glc} (black) and phosphorylated EIIA^{Glc} by EI in the absence of HPr (green). c) Overlay of 2D spectra for the phosphorylated EIIA^{Glc} in the presence (red) or absence of HPr (green). d) EIIA^{Glc} phosphorylation results in large chemical shift perturbations (CSPs) that can be mapped to the vicinity of the active site residue, H90. The perturbed residues are colored blue.

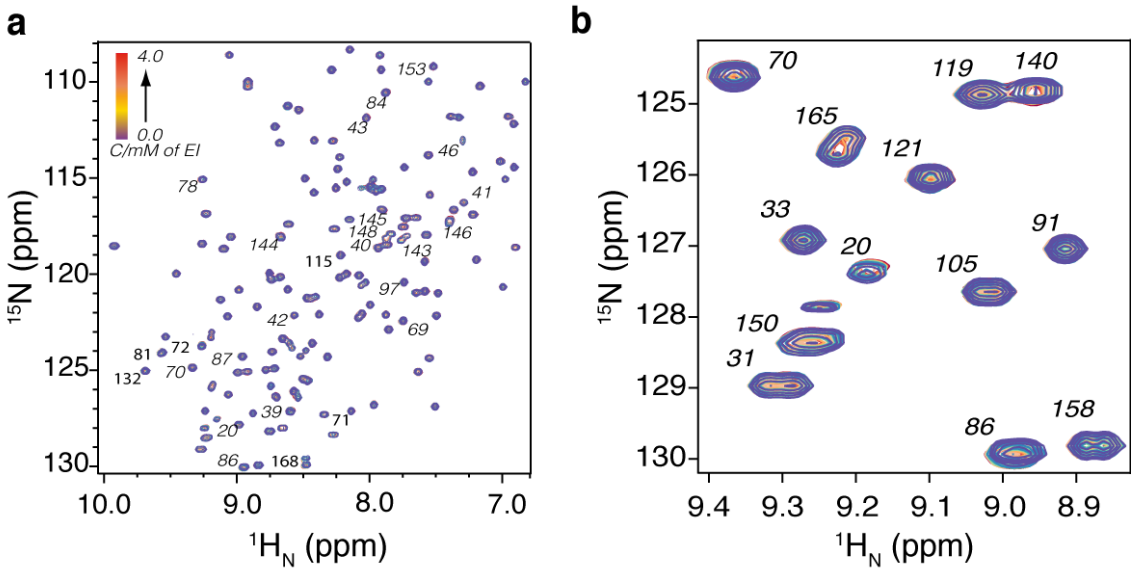

Figure S2. NMR chemical shift perturbations of ^{15}N-labeled EIIA^{Glc} titrated with full-length EI up to 4 mM. Residues with putative CSPs are labeled, and the same zoom-in area of the 2D spectrum was shown in (**b**) as in **Figure 1a**.

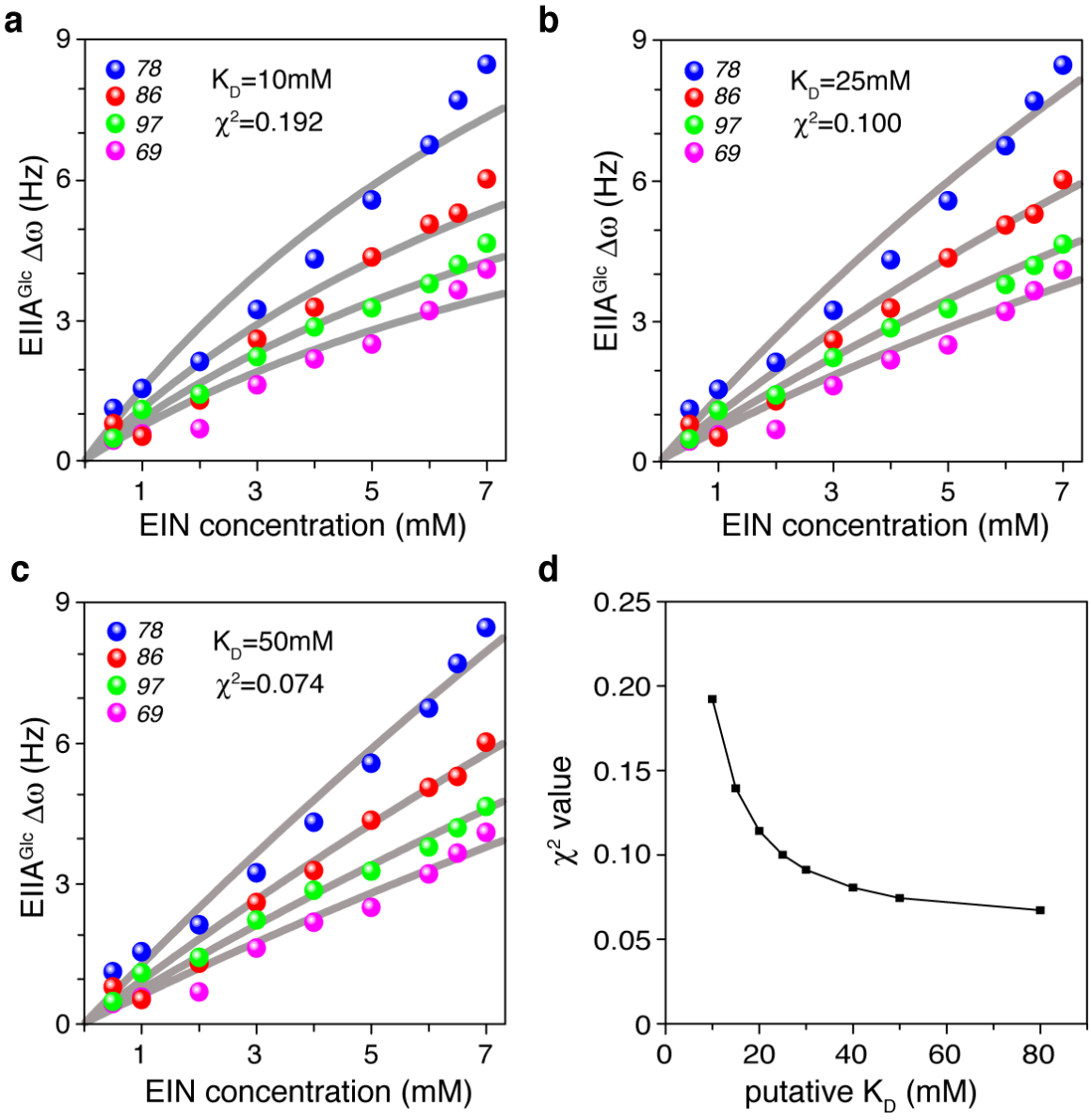

Figure S3 Fitting of chemical shift perturbations with putative K_D values. CSPs for residues 69, 70, 78, 86 and 97 of $EIIA^{Glc}$ are fitted to theoretical curves with (**a**) K_D = 10 mM, (**b**) K_D = 25 mM and (**c**) K_D = 50 mM, affording residual χ^2 values of 0.192, 0.100 and 0.074, respectively. (**d**) Residual χ^2 values from fitting $EIIA^{Glc}$ CSPs are plotted over putative K_D. The χ^2 value levels off with K_D value of 25 mM or larger.

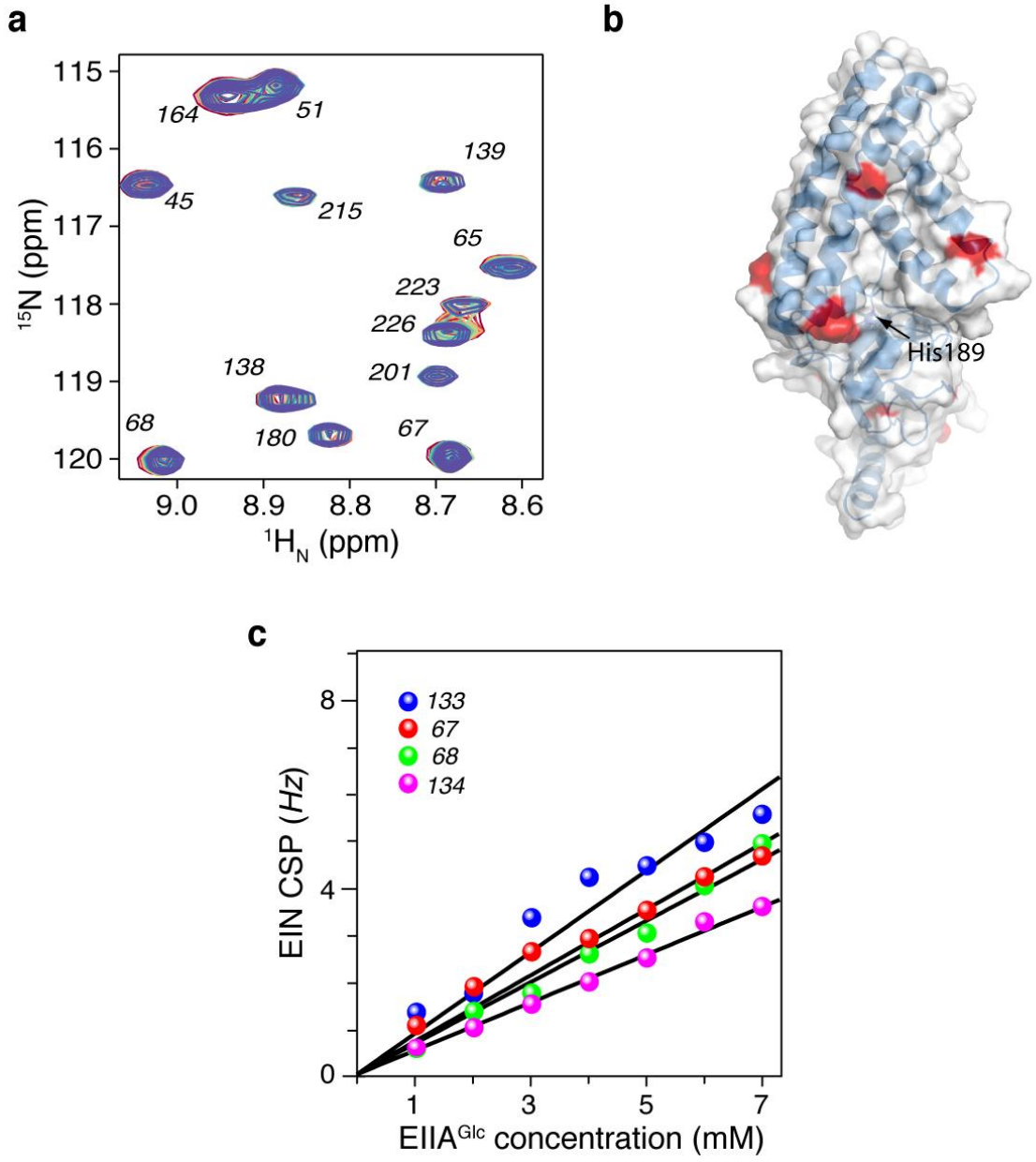

Figure S4. NMR chemical shift perturbations of EIN upon $EIIA^{Glc}$ titration. (**a**) Overlay of a region of 2D ^{1}H-^{15}N correlation spectra by titrating up to 7 mM of $EIIA^{Glc}$ into 1 mM of ^{15}N-labeled EIN, respectively. (**b**) Residues with chemical shift perturbations > 3Hz are mapped onto the surface EIN structures. (**c**) CSPs are plotted over titrant concentrations for $EIIA^{Glc}$.

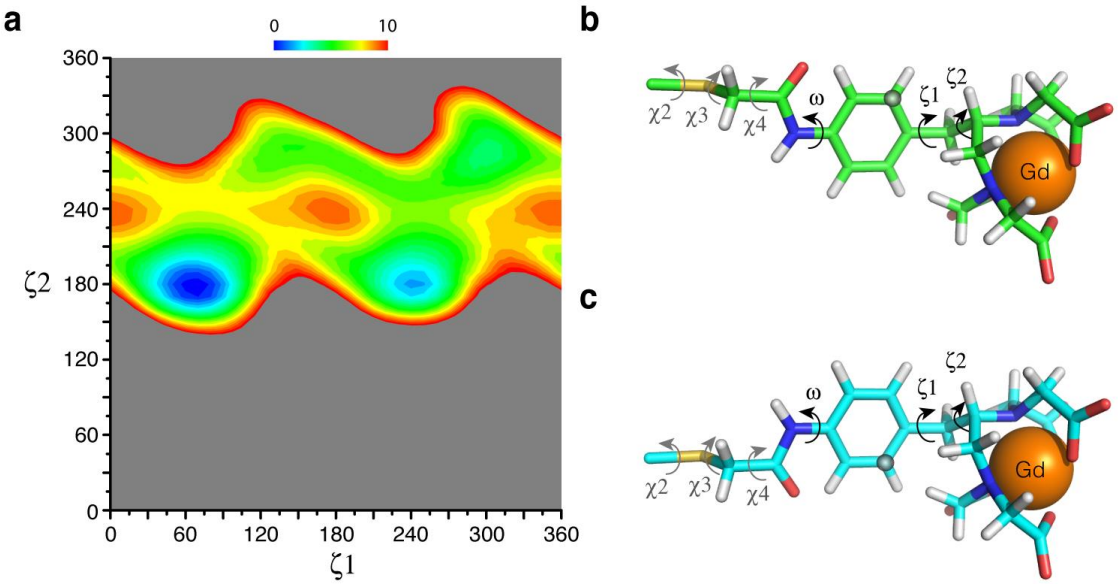

Figure S5. Conformational space for cysteine-conjugated Gd^{3+}-EDTA-benzyl-acetate paramagnetic probe. (**a**) Energy landscape was computed with B3LYP/6-31G* scheme using Gaussian 09 (Gaussian, Inc.), by incrementing the dihedral angles ζ1 and ζ2 every 10º. The ζ1 and ζ2 angles are defined in (**b**) and (**c**). The heat map scales from 0 to 10 KCal/mol, with 0.08 KCal/mol at the lowest point; (ζ1, ζ2) combinations that have energies greater than 10KCal/mol are colored in grey. (**b**,**c**) The two configurations of the paramagnetic probe that have the lowest energies, corresponding to (ζ1, ζ2) angles of (60º, 180º) and (240º, 180º). The two configurations differ by an 180º rotation of the benzyl ring relative to the EDTA moiety, i.e. ζ1 = 60º or ζ1 = 240º. As the dihedral angle ω for the peptide bond can either be in *syn* or *anti* configuration, i.e. ω = 0º or ω = 180º, this is equivalent to ζ1 angle flipping between 60º and 240º. The two configurations are located at the steepest portion of the (ζ1, ζ2) plot, while configurations outside the basin encounter large steric clashes and are energetically unfavorable. Thus, we fixed (ζ1, ζ2) angles and treated these two configurations as two different probes in the PRE calculation, allowing only χ1, χ2, χ3 and χ4 angles to freely rotate (χ1 angle to the backbone Cα atom not shown in the figure). Precursor to the paramagnetic probe, (S)-1-(p-bromo-acetamido-benzyl) ethylene-diamine tetra-acetate, CAS number 81677-64-7, was purchased from Toronto Research Chemicals and was reacted with the protein as described in the Methods.

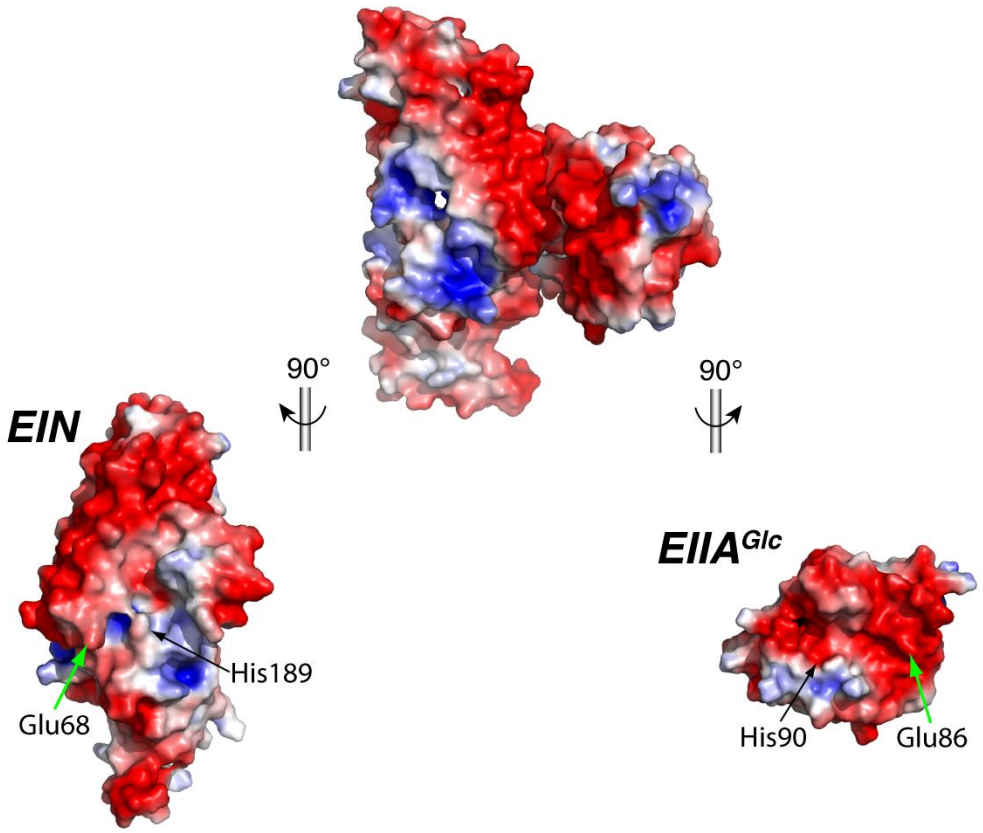

Figure S6. Solvent accessible surface of EIN-EIIA^{Glc} complex colored by the electrostatic potential. The electrostatic potential is calculated with APBS tool[22] in the presence of 100mM NaCl at pH 7.2 and 310 K in PyMOL, plotted over a scale from -3 kT to 3 kT, and colored from red (negative) to blue (positive) on protein surface. The two separate illustrations for EIN and EIIA^{Glc} are related to their perspective in the fleeting complex by a 90° rotation, thus to show the electrostatic potential at the buried interface. Besides the active site histidines, EIN residue Glu68 and EIIA^{Glc} residue Glu86 are indicated.

Table S1 Structural statistics of the EIN-EIIA^{Glc} complex [a]

	<SA>	<SA$_{phos}$>
Number of experimental restraints		
Intermolecular PRE restraints [b]	473	473
Distance restraints [c]	14	14
Deviation from experimental restraints		
PRE restraints (s^{-1})	2.99 ± 0.05	2.98 ± 0.01
Distance restraints (Å)	0.01 ± 0.01	0.01 ± 0.01
Deviation from idealized covalent geometry [d]		
Bond lengths (Å)	0.00 ± 0	0.00 ± 0
Bond angles (º)	0.45 ± 0	0.47 ± 0
Improper angles (º)	1.79 ± 0	1.81 ± 0
Measurement of structural quality		
Intermolecular repulsion energy (kcal/mol) [e]	0.16 ± 0.21	1.11 ± 0.82
Interfacial compactness energy (kcal/mol) [f]	65.0 ± 2.0	57.8 ± 0.97
Coordinate precision of the complex (Å) [g]		
Backbone (N, Cα, C', O) atoms	0.74 ± 0.21	0.34 ± 0.12
Including side-chain heavy atoms	0.99 ± 0.17	0.68 ± 0.07

a. Analyses were performed on <SA> the final 69 simulated annealing structures of the EIN-EIIA^{Glc} complex and <SA$_{phos}$> 74 structures for phosphorylation transition state, each from 128 starting structures calculated.

b. Comprising 135, 135 and 213 restraints, with the paramagnetic probe attached at EIN E63C, EIN E117C and EIIA^{Glc} E43C site, respectively.

c. H-bond restraints for the regular secondary structures near the active site histidines.

d. Additional covalent restraints were applied to calculate the phosphorylation transition-state complex by enforcing a trigonal bipyramidal geometry of the phosphoryl group: r(Nε2-P) ≤ 3.5 Å, Nε2-P-O = 90º, and improper(Nε2-P-Cε1-Cδ2) = 0º to ensure the phosphorus atom is coplanar with the imidazole rings of active site histidines of both EIN His189 and EIIA^{Glc} His90.

e. Quartic repulsive term was calculated with van der Waals force constant of 4 kcal•mol^{-1}•Å^{-4} and van der Waals radius scaling factor of 0.75.

f. To ensure the compactness of the complex, a radius-of-gyration restraint was applied to the entire complex[23] and to the protein interface as mapped from NMR titration,[9] with the target value set as 2.2×N^0.38, where N is the number of residues involved. The putative interface includes EIN residues 59, 68-69, 82 and 118 and EIIA^{Glc} residues 40-46, 69-70, 78, 84-87, 97, 143-149. Collapse energy terms for radius-of-gyration pseudopotential were reported.

g. The r.m.s. differences of the ensemble relative to the mean coordinates, which was obtained by first superimposing all backbone heavy atoms of the complex in the ensemble.

Supplementary references

[1] P. Schanda, B. Brutscher, *J. Am. Chem. Soc.* **2005**, *127*, 8014-8015.

[2] K. A. Datsenko, B. L. Wanner, *Proc. Natl. Acad. Sci. USA* **2000**, *97*, 6640-6645.

[3] T. Durfee, R. Nelson, S. Baldwin, G. Plunkett, 3rd, V. Burland, B. Mau, J. F. Petrosino, X. Qin, D. M. Muzny, M. Ayele, R. A. Gibbs, B. Csorgo, G. Posfai, G. M. Weinstock, F. R. Blattner, *J. Bacteriol.* **2008**, *190*, 2597-2606.

[4] T. M. Rana, C. F. Meares, *J. Am. Chem. Soc.* **1990**, *112*, 2457-2458.

[5] J. Iwahara, C. D. Schwieters, G. M. Clore, *J. Am. Chem. Soc.* **2004**, *126*, 5879-5896.

[6] C. D. Schwieters, J. J. Kuszewski, G. M. Clore, *Prog. Nucl. Magn. Reson. Spectrosc.* **2006**, *48*, 47-62.

[7] D. I. Liao, E. Silverton, Y. J. Seok, B. R. Lee, A. Peterkofsky, D. R. Davies, *Structure* **1996**, *4*, 861-872.

[8] M. D. Feese, L. Comolli, N. D. Meadow, S. Roseman, S. J. Remington, *Biochemistry* **1997**, *36*, 16087-16096.

[9] C. Tang, G. M. Clore, *J. Biomol. NMR* **2006**, *36*, 37-44.

[10] I. Bertini, C. Luchinat, S. Aime, *Coord. Chem. Rev.* **1996**, *150*, 77-110.

[11] G. M. Clore, C. D. Schwieters, *J. Am. Chem. Soc.* **2003**, *125*, 2902-2912.

[12] J. Kuszewski, A. M. Gronenborn, G. M. Clore, *Protein Sci.* **1996**, *5*, 1067-1080.

[13] a) J. G. Pelton, D. A. Torchia, S. J. Remington, K. P. Murphy, N. D. Meadow, S. Roseman, *J. Biol. Chem.* **1996**, *271*, 33446-33456; b) D. S. Garrett, Y. J. Seok, A. Peterkofsky, G. M. Clore, A. M. Gronenborn, *Biochemistry* **1997**, *36*, 4393-4398.

[14] Y. S. Jung, M. Cai, G. M. Clore, *J. Biol. Chem.* **2012**, *287*, 23819-23829.

[15] G. Wang, J. M. Louis, M. Sondej, Y. J. Seok, A. Peterkofsky, G. M. Clore, *EMBO J.* **2000**, *19*, 5635-5649.

[16] N. Homeyer, A. H. Horn, H. Lanig, H. Sticht, *J. Mol. Model.* **2006**, *12*, 281-289.

[17] D. A. Case, T. A. Darden, T. E. I. Cheatham, C. L. Simmerling, J. Wang, R. E. Duke, R. Luo, R. C. Walker, W. Zhang, K. M. Merz, B. Roberts, S. Hayik, A. Roitberg, G. Seabra, J. Swails, A. W. Goetz, I. Kolossváry, K. F. Wong, F. Paesani, J. Vanicek, R. M. Wolf, J. Liu, X. Wu, S. R. Brozell, T. Steinbrecher, H. Gohlke, Q. Cai, X. Ye, J. Wang, M. J. Hsieh, G. Cui, D. R. Roe, D. H. Mathews, M. G. Seetin, R. Salomon-Ferrer, C. Sagui, V. Babin, T. Luchko, S. Gusarov, A. Kovalenko, P. A. Kollman, *AMBER 12* **2012**.

[18] D. Hamelberg, J. Mongan, J. A. McCammon, *J. Chem. Phys.* **2004**, *120*, 11919-11929.

[19] a) C. A. de Oliveira, B. J. Grant, M. Zhou, J. A. McCammon, *PLoS Comput. Biol.* **2011**, *7*, e1002178; b) L. C. Pierce, R. Salomon-Ferrer, F. d. O. C. Augusto, J. A. McCammon, R. C. Walker, *J. Chem. Theory Comput.* **2012**, *8*, 2997-3002.

[20] K. Aoki, K. Takahashi, K. Kaizu, M. Matsuda, *Scientific Rep.* **2013**, *3*, 1541.

[21] G. Schreiber, G. Haran, H. X. Zhou, *Chem. Rev.* **2009**, *109*, 839-860.

[22] N. A. Baker, D. Sept, J. S., M. J. Holst, J. A. McCammon, *Proc. Natl. Acad. Sci. U. S. A.* **2001**, *98*, 10037-10041.

[23] J. Kuszewski, A. M. Gronenborn, G. M. Clore, *J. Am. Chem. Soc.* **1999**, *121*, 2337-2338.